International Journal of Greenhouse Gas Control 112 (2021) 103511

Contents lists available at ScienceDirect

International Journal of Greenhouse Gas Control

journal homepage: www.elsevier.com/locate/ijggc

The impact of heterogeneity on the capillary trapping of CO_2 in the Captain Sandstone.

Catrin Harris [a,*], Samuel J. Jackson [b], Graham P. Benham [c,d], Samuel Krevor [a], Ann H. Muggeridge [a]

[a] Department of Earth Science and Engineering, Imperial College London, London, UK
[b] CSIRO Energy, Clayton South, Victoria, Australia
[c] Department of Earth Sciences, University of Cambridge, Cambridge, UK
[d] Centre for Environmental and Industrial Flows, University of Cambridge, Cambridge, UK

ARTICLE INFO

Keywords:
CO_2 Sequestration
Capillary trapping
Heterogeneity
Imbibition

ABSTRACT

A significant uncertainty which remains for CO_2 sequestration, is the effect of natural geological heterogeneities and hysteresis on capillary trapping over different length scales. This paper uses laboratory data measured in cores from the Goldeneye formation of the Captain D Sandstone, North Sea in 1D numerical simulations to evaluate the potential capillary trapping from natural rock heterogeneities across a range of scales, from cm to 65m. The impact of different geological realisations, as well as uncertainty in petrophysical properties, on the amount of capillary heterogeneity trapping is estimated. In addition, the validity of upscaling trapping characteristics in terms of the Land trapping parameter is assessed. The numerical models show that the capillary heterogeneity trapped CO_2 saturation may vary between 0 and 14% of the total trapped saturation, depending upon the geological realisation and petrophysical uncertainty. When upscaling the Land model from core-scale experimental data, using the maximum experimental Land trapping parameter could increase the expected heterogeneity trapping by a factor of 3. Conversely, depending on the form of the imbibition capillary pressure curve used in the numerical model, including capillary pressure hysteresis may reduce the heterogeneity trapping by up to 70%.

1. Introduction

A major challenge for geological carbon storage is increasing confidence in trapping mechanisms which do not depend on structural closures within the reservoir The IPCC special report on carbondioxide capture and storage (2006). Post CO_2 injection, secondary trapping mechanisms become increasingly important to storage security Benson (2012). Residual trapping, whereby isolated ganglia of CO_2 are trapped by capillary forces within a single rock pore, or across a few pores, is a key mechanism underpinning security and immobilizing a significant proportion of the CO_2 plume Krevor et al. (2015). In some estimates it underpins more than 90% of geological storage resources Blondes et al. (2013). The physics and modelling of pore scale residual trapping is well established Krevor et al. (2015). On injection, CO_2 migrates through the aquifer giving rise to brine imbibition into the pore space at the trailing edge of the CO_2 plume Benson (2012). Laboratory and field experiments have identified that the saturation of pore-scale residually trapped CO_2, $S_{CO_2,r}$, is proportional to the maximum initial CO_2 saturation achieved prior to brine imbibition, $S_{CO_2,i}$ Land (1968); Ni et al. (2019). The Land trapping model is one of the most widespread models used to describe this relationship,

$$S_{CO_2,r} = \frac{S_{CO_2,i}}{1 + CS_{CO_2,i}}, \quad (1)$$

where C is an empirical constant characterising the trapping strength Krevor et al. (2012), with values typically within the range 1–2 for sandstones from pilot CO_2 storage sites Dance and Paterson (2016); Krevor et al. (2015). The relationship is characteristic of the rock pore structure, making it specific to the reservoir Krevor et al. (2015). For homogeneous water wet rocks, the Land model has been demonstrated to be a good match with experiments Jackson and Krevor (2020).

* Corresponding author.:.
E-mail addresses: c.harris19@imperial.ac.uk (C. Harris), samuel.jackson@csiro.au (S.J. Jackson), gpb35@cam.ac.uk (G.P. Benham), s.krevor@imperial.ac.uk (S. Krevor), a.muggeridge@imperial.ac.uk (A.H. Muggeridge).

https://doi.org/10.1016/j.ijggc.2021.103511
Received 13 May 2021; Received in revised form 5 September 2021; Accepted 21 October 2021
Available online 6 November 2021

In recent years a trapping mechanism has been identified in which capillary forces acting at cm-m scales result in the local immobilization of CO_2 upstream of heterogeneities in the reservoir Krevor et al. (2015); Saadatpoor et al. (2010). Capillary pressure heterogeneities give rise to baffles throughout the domain, resulting in the accumulation of CO_2 as a continuous locally trapped phase upstream of regions of high capillary pressure Bech and Frykman, 2018; Krevor et al. (2011); Saadatpoor et al. (2010). The heterogeneity causes a capillary pressure gradient which effectively stops this accumulated CO_2 from desaturating, so more CO_2 is immobilized than what would have occurred due to the pore scale trapping mechanism alone Bech and Frykman, 2018. Capillary heterogeneity trapping has been identified in both simulation-based work and through experimental observations Bech and Frykman, 2018; Gershenzon et al. (2017); Jackson et al. (2020); Krevor et al. (2011); Ni et al. (2019); Obi and Blunt, 2006; Pini and Benson (2017); Reynolds et al., 2018; Saadatpoor et al. (2010). These studies identify that capillary heterogeneities impact plume migration dynamics and can account for over 50% of CO_2 trapped within the reservoir rock. Capillary trapping relationships on both the core and field scale have been shown to be sensitive to the impact of geological heterogeneity Dance and Paterson (2016).

A number of uncertainties regarding the physics and impacts of capillary heterogeneity trapping remain Bech and Frykman, 2018; Gershenzon et al. (2017, 2014). These include the impact of flow conditions and geological settings; the relative importance of pore-scale residual trapping and the larger scale heterogeneity trapping; and approaches to characterising storage sites so the impacts of heterogeneity trapping may be represented in reservoir models. The impact of capillary pressure hysteresis also remains a major uncertainty, with many previous studies omitting capillary pressure hysteresis due to long simulation run times Bech and Frykman, 2018; Saadatpoor et al. (2010).

This paper characterises the role of capillary heterogeneity trapping within a target storage site, the Goldeneye Field of the Captain D Sandstone. We have carried out steady-state core flooding experiments using medical x-ray CT scanning on a sample set of composite cores taken from a 65m height interval of the Captain Sandstone. The analysis provides a detailed characterisation of continuum multiphase flow properties, including residual trapping characteristics, over cm-scales. Numerical models are constructed from observations of residual trapping in heterogeneous rock cores Jackson et al. (2018); Jackson and Krevor (2020) to evaluate the impact of layered heterogeneities on trapping as we approach the field scale. These models aim to resolve uncertainties in existing literature by studying the impact of capillary heterogeneity trapping over a range of flow conditions and geological realisations for the Captain Sandstone. The workflow and results are also applicable to many other storage sites of similar geology, for example layered sandstone units in the North Sea such as the Endurance Field and Sleipner Field Chadwick et al., 2009; Metcalfe et al. (2017).

2. Captain Sandstone - experimental data

The Goldeneye formation in the Captain Sandstone, UK North Sea, represents a typical CO_2 storage unit, an aquifer in an unconsolidated sandstone Spence et al., 2014. The Captain Sandstone was the target industrial injection site for the discontinued Peterhead CCS project, with the aim to store 10 Mt CO_2 over 10 years Spence et al., 2014. Due to its potential as a CO_2 storage site, the Captain Sandstone has been the subject of several recent investigations Jackson and Krevor (2020); Jin et al. (2012); Reynolds et al., 2018. Of particular relevance here is the work of Jackson and Krevor (2020) which characterised experimentally the drainage flow properties over a 65m interval of the Captain Sandstone. We build on that work by analysing the imbibition processes, experimentally characterising initial-residual trapping relationships.

The following section summarizes the core analysis data used to create 1D field-scale numerical models of the Goldeneye Field. We incorporate the experimental data from Jackson and Krevor (2020), in addition to publicly-available data for well 14/29a-3, collected by Shell during the Peterhead FEED project Shell (2015). For the experimental methods used to determine the capillary pressure and relative permeability functions for the Captain Sandstone see Jackson and Krevor (2020).

2.1. Capillary pressure and relative permeability

The Brooks Corey model Brooks and Corey (1964) is used to parameterise the relationship between capillary pressure P_c and wetting phase saturation S_w,

$$P_c = P_e S_w^{*\,-1/\lambda}, \tag{2}$$

$$S_w^* = \frac{S_w - S_{wirr}}{1 - S_{wirr}}, \tag{3}$$

where P_e is the capillary entry pressure, S_w* is the wetting phase saturation normalised with respect to the irreducible water saturation S_{wirr} and λ is the pore-size distribution factor. At steady state, the macroscopic capillary pressure function is approximately constant through the core Jackson et al. (2020).

Mercury intrusion porosimetry (MIP) was carried out on 13 plugs, in order to obtain the capillary pressure - saturation relationships Jackson and Krevor (2020). The parameters in Eq. (2)– were fitted using orthogonal distance regression, resulting in $\lambda = 0.75$ and $P_e = 39.59$ kPa for mercury/air system, scaled to $P_e = 2.69$ kPa for the CO_2/brine system using the ratio of interfacial tensions Benson et al. (2013); Li et al. (2012); Pini and Benson (2013). $S_{wirr} = 0.12$ in all plugs, implying similar wettability and displacement conditions Pini and Benson (2013). The experimental imbibition capillary pressure - saturation relationship was not measured and should be the subject of future investigations.

The Leverett J-function (Eq. 4) was used to scale the MIP capillary pressure data with porosity ϕ and permeability K data from poroperm experiments Leverett (1940), with the interfacial tension $\gamma = 33$ mN/m and contact angle $\theta = 50°$ for CO_2-brine Jackson and Krevor (2020). See (Jackson, Krevor, 2020) for further details of the experimental procedure . Capillary pressure data collapses onto a single function fitted with the Brooks Corey model (Fig. 1a). The model is a good fit to the data therefore validating the assumption of universal relative permeability curves over the domain as per Burdine's theory (Li and Benson, 2015).

$$J = \frac{P_c}{\gamma \cos(\theta)} \sqrt{\frac{K}{\phi}} \tag{4}$$

The composite average drainage relative permeability of each phase was calculated through the multiphase extension of Darcy's law, using the pressure drop across the core determined from steady-state core floods Jackson and Krevor (2020). The intrinsic drainage relative permeability - saturation relationships are parameterised using Chierici functions Eqs. (5) and (6) Chierici (1984) by Jackson and Krevor (2020), with $k_{rw}{}^e = 1$, $k_{rg}{}^e = 0.6$, A = 6.3, B = 1.9, M = 1.3, L = 1. The connate gas saturation, $S_{gc} = 0$ Jackson and Krevor (2020).

$$k_{rw} = k_{rw}^e e^{-AR_w^{-L}} \tag{5}$$

$$k_{rg} = k_{rg}^e e^{-BR_w^M} \tag{6}$$

$$R_w = \frac{S_w - S_{wirr}}{1 - S_{gc} - S_w} \tag{7}$$

Imbibition CO_2 relative permeability (Fig. 1b) is calculated by implementing conventional methods using the mobile, connected CO_2 saturation, based on residual trapping relationships Jackson et al. (2020). In this example the Land trapping model (Eq. 1) is used to define pore-scale residually trapped CO_2 saturation and therefore hysteresis.

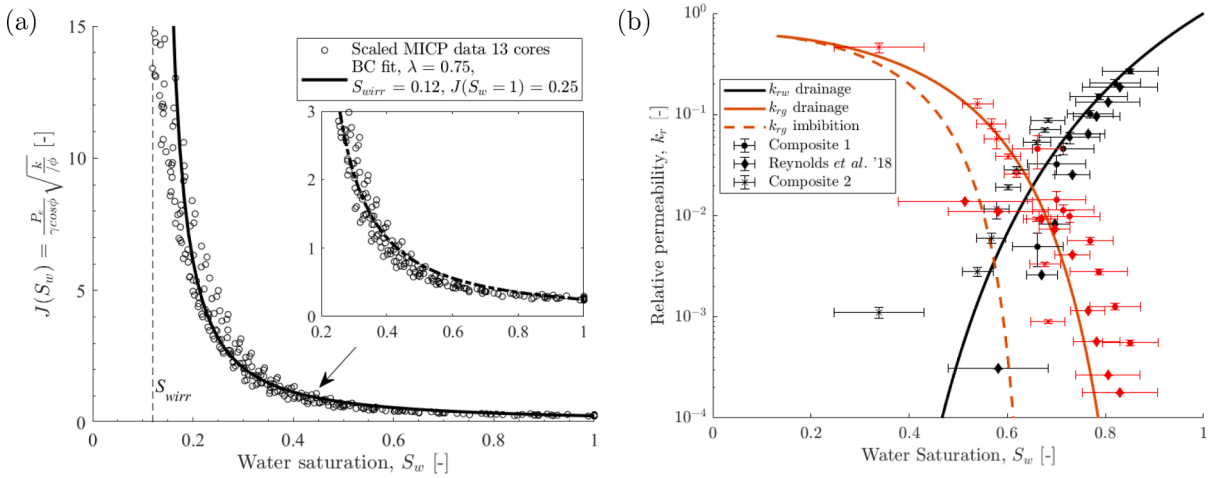

Fig. 1. (a.) MIP data for 13 plugs scaled by the Leverett J-function with poroperm measured porosity and permeability, and fitted with the Brooks Corey model. Direct from Jackson and Krevor (2020). (b.) Chierici relative permeability curves fitted to experimental data for the Captain sandstone, with associated uncertainty from Jackson and Krevor (2020). The CO_2 imbibition relative permeability curve is calculated from the mobile CO_2 saturation.

Table 1
Base parameters used in the simulations. Other parameters such as flow rate and geological realisation are varied.

System size	65 m
Temperature	80 °C
Average Pressure	15500 kPa
ρ_w	1023 kg/m^3
ρ_{CO_2}	694 kg/m^3
μ_{CO_2}	0.0570 mPas
μ_w	0.4060 mPas

2.2. Initial-Residual relationships

Steady-state core flooding experiments were performed using medical x-ray CT scanning to characterise residual trapping characteristics at the cm-scale. Four composite cores were tested, consisting of 5 or 6 individual plugs from distinct locations, with average composite depths 2554 m, 2564 m, 2576 m and 2604 m, chosen to compliment the existing dataset obtained on a composite core at depth 2562.7–2568.7 m by Reynolds et al., 2018. Nitrogen-water (DI water or 1 molal NaCl brine) core-floods were performed at elevated pressure (10 MPA pore-pressure) and ambient temperatures (19.5 °C ± 0.3 °C composite 1, 18.6 °C ± 0.7 °C composite 2, 17.6 °C ± 0.4 °C composite 3, 17.7 °C ± 0.5 °C composite 4) using the experimental setup and methodology detailed in Reynolds and Krevor (2015). Nitrogen was used as an experimental analog to supercritical CO_2 Jackson and Krevor (2020); Krevor et al. (2012). For composites 2, 3 and 4 DI water was used as the wetting phase, whilst for the more mudstone/clay rich composite 1 we used 1 Molal NaCl brine, to limit swelling. Using the set-up outlined in Jackson and Krevor (2020), the following workflow was carried out:

1. To drain the core, 100% nitrogen was injected at 20 mL.min^{-1}. From the final conditions of step 15 outlined in the Supporting Information Jackson and Krevor (2020), the proportion of nitrogen was increased to 100% to complete the drainage fractional flow regime. Some measurements previously underwent an imbibition fractional flow regime, before 100% nitrogen was injected.
2. Once steady-state had been reached, at least three full core, partially saturated scans were taken.
3. The nitrogen flow was stopped and 100% working fluid water (DI water or brine) was injected into the core at 20 mL.min^{-1}.

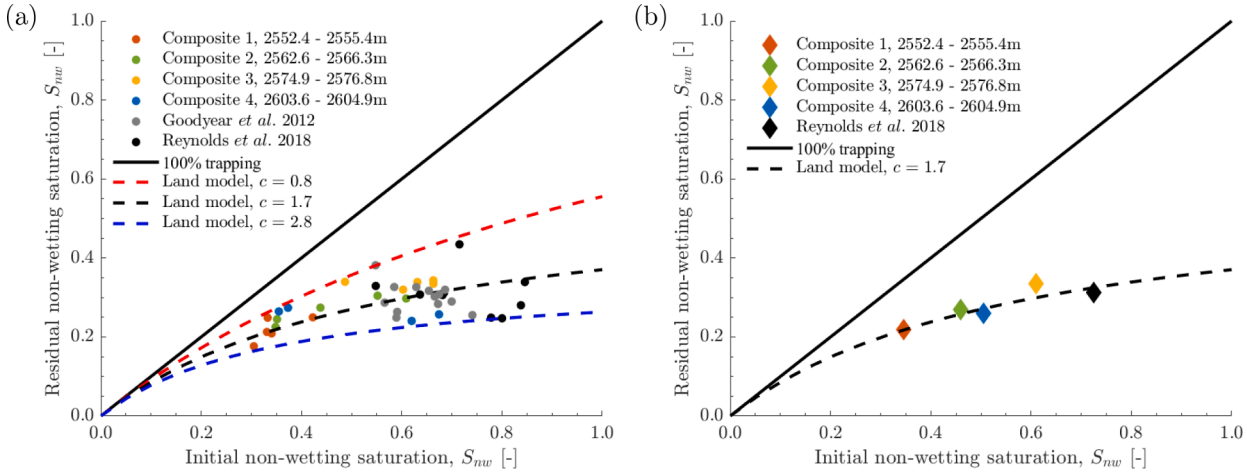

Fig. 2. Initial-residual saturation plots illustrating trapping characteristics for different Captain Sandstone (a.) plug and (b.) core averages, alongside data from literature Boom et al. (2012); Reynolds et al., 2018. The 1:1 line demonstrates 100% trapping, where all initial CO_2 saturation is retained. The average Land trapping parameter at the plug scale is calculated as 1.7, using least squared regression. The maximum and minimum Land trapping curves are defined by the Land trapping parameter for which all the data falls above or below the respective Land trapping curve.

4. Once brine was observed to have passed through the core, full core scans were taken. Scans were taken when the saturation had reached a steady-state, and nitrogen dissolution effects were negligible

Individual plug and composite average initial-residual saturation relationships were created by comparing the saturations prior to and post imbibition injection of the wetting-phase working fluid (see Supporting Information S1 for voxel saturations). The results, Fig. 2, show that individual core plugs exhibit a large range in apparent residual trapping at the cm-scale (Fig. 2a), which when averaged over the core scale of 10s of cm's or greater collapse onto the same curve (Fig. 2b). The average Land trapping value at the deca-centimetre scale is 1.7, however, at the cm-scale, it varies between 0.8 and 2.8, indicating a large variation in locally trapped CO_2 due to variations in pore connectivity, and the connectivity and length scale of capillary heterogeneities Krevor et al. (2015). At the plug-scale, for large initial saturations the average residual saturation may vary between 0.2 and 0.5. At lower initial saturations, the variations at the plug scale are not as great in absolute terms, but the relative variation is just as large, falling within the same range of Land trapping parameters.

2.3. Field-scale data

The porosity (ϕ) - permeability (K) relationship established in Jackson, Krevor, (2020) for the Captain Sandstone was used to calculate the permeabilities of the different layers in the model, from the corresponding log porosities,

$$\ln K = 52.54\phi - 6.47 \tag{8}$$

where permeability K is measured in mD Jackson and Krevor (2020). The relationship was extracted from routine core analysis (RCAL) data collected by Shell (2015) and Jackson and Krevor (2020).

3. Assessment of geological and petrophysical uncertainties

It is well known that uncertainty in heterogeneity can have a large impact on modelling predictions of plume migration Jackson et al. (2018); Jackson and Krevor (2020); Reynolds et al., 2018, and more recently Mathias et al., 2013 have shown relative permeability uncertainty impacts CO_2 injectivity. In this section we briefly outline the key sources of uncertainty related to estimating capillary heterogeneity trapping, over the decametre scale in the Captain D sandstone, using numerical flow simulation, and how we quantify each of these. The three uncertainties considered are:

1. Uncertainty due to the ordering and properties of the layers, resulting from natural geological heterogeneity.
2. Uncertainty due to limited vertical resolution in the wireline log data. In particular, very thin layers (less than approximately 0.5m thick Tiab and Donaldson (2016)) that are not captured by the log measurements may nevertheless have a significant effect on capillary trapping.
3. Uncertainty in the empirical relationships for the intrinsic rock-fluid properties (such as porosity, permeability, relative permeability and capillary pressure), as often experimental measurements of such properties have a large degree of scatter, or are inferred from other uncertain measurements.

3.1. Generating geological model realisations

Since heterogeneity data are often sparse or incomplete, it is useful to model a variety of likely realisations, rather than focusing on the implications of a single modelling prediction. To investigate uncertainty due to natural geological heterogeneity, we created multiple realisations of layering, perpendicular to flow, in a 1D vertical section of the reservoir. The models are built from the statistical properties of the measured wireline log data detailed in Shell U.K. reports Shell (2015) for the Captain D sandstone interval (true vertical depth, *TVD* 2525-2590m), the planned injection interval for the Peterhead CCS project (Tucker and Tinios, 2017).

First, frequency distributions of the porosity and layer thicknesses were determined from wireline log data. From these distributions layer widths and porosity values were sampled independently, using inverse transform sampling Devroye (1986). To generate the porosity distribution, the porosity-depth trend (ϕ = -0.0003TVD + 1.01) was subtracted from the Shell wireline log data Jackson and Krevor (2020) to obtain a stationary dataset suitable for statistical analysis (Fig. 3a). Once a porosity-depth realisation had been sampled, the porosity-depth trend was re-imposed, allowing the porosity-depth trend to be properly accounted for in the model (see Supporting Information S2).

To study the impact of 1D geological heterogeneities within the Captain Sandstone, layers are approximated to describe features such as bedding planes. To calculate the probability density function (PDF) for the layer structure, we first needed to identify layers from the vertical permeability data derived from the Shell wireline log data Shell (2015) and Eq. (8). An optimisation approach implementing a set of smooth tanh functions was employed, by which an optimum set of layer thicknesses and layer permeabilities were found. To do this, we fitted a series of hyperbolic tangent functions of the form

$$K(z) = K_1 + \sum_{j=1}^{n-1} \left[\frac{K_{j+1} - K_j}{2} \left(1 + \tanh\left(\frac{z - w_j}{\epsilon} \right) \right) \right] \tag{9}$$

to the measured permeability profile $k(z)$, where $\epsilon << w_j$ is a small smoothing parameter, w_j are the fitted vertical locations of the different layers j and K_j are the permeability values within those layers, which are simply taken as the mean

$$K_j = \frac{1}{w_j - w_{j-1}} \int_{w_{j-1}}^{w_j} k(z) dz. \tag{10}$$

Using a least squares optimisation procedure, we fitted the width positions w_j to the measured data, assuming a total number of layers n. We chose n large enough such that all of the layers were captured by Eq. (9), but not so large that we ended up with redundant layer width parameters w_j (see Supporting Information S3). Under these criteria, the measured data $k(z)$ were well approximated by Eq. (9) with n = 40 layers, as illustrated in Fig. 3c. The fitted layer widths $\delta z_j = w_j - w_{j-i}$ varied between 1% and 5% of the total vertical scale. The probability density function of layer widths is approximately uniform (Fig. 3b), indicating that there is no predominant length-scale for sediment deposition in this sandstone. There is no correlation between the width of the layers and their vertical location, nor their permeability values (see Supporting Information S3). However, as discussed earlier, there is a trend between permeability and depth. Hence $\{\delta z_j, z_j\}$ are taken as independent variables, as are $\{\delta z_j, K_j\}$, but $\{z_j, K_j\}$ are correlated.

Porosity values and layer width values were sampled independently from the depth-independent porosity distribution and uniform layer width distribution respectively. The different realisations consisted of 40 layers on average. Realisations of porosity-depth were converted to capillary entry pressure-depth, scaled using the Leverett-J function, Eq. (4) Leverett (1940). This gave us a spread of different capillary trapping predictions based on the different realisations of the Goldeneye Field, from which we inferred useful metrics such as the mean trapping and standard deviation.

3.2. Uncertainty due to wireline log resolution

To investigate the effect of uncertainty due to finite resolution in the vertical coordinate, we repeated the above procedure, except we

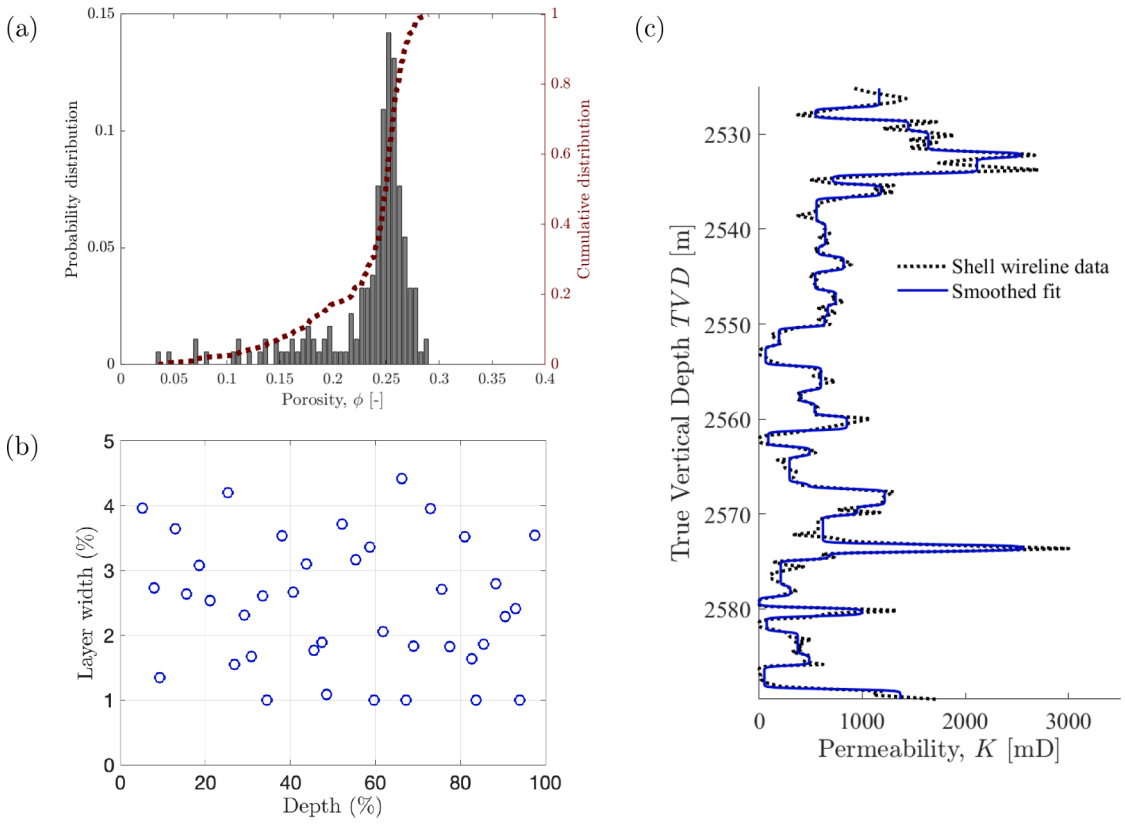

Fig. 3. (a.) Porosity histogram and cumulative distribution function fitted to Shell wireline log data Jackson and Krevor (2020) for the Captain D sandstone, following the subtraction of the depth-trend. (b.) Layer width distribution as a function of interval depth. (c.) The permeability - depth relationship derived from Shell wireline log data (well 14/29a-3) is fitted with a smooth tanh function approximation (Eq. 9) in order to create distributions of layer thicknesses and layer permeabilities Shell (2015).

extended the uniform distribution down to a cut-off length-scale $\delta_{\min} = 0$ m. Since no information is known about layers of width smaller than 1% of the total vertical length-scale, we had to extrapolate the PDF. Whilst there are many possible ways of doing this, for the purpose of simplicity we set the PDF for $\delta z_j \in [0, 1]$% as the mean value of the whole distribution, with the new PDF normalised appropriately. We draw layer widths from the probability density function extended to account for sub-resolution layers (instead of the original one) and repeated our modelling calculations. Then, the difference between the mean predictions for the original PDF and the mean for the extended PDF provides a metric for the potential uncertainty due to sub-resolution heterogeneities.

3.3. Uncertainty in multiphase petrophysical properties

In the context of this paper, experimental measurements were used to determine the relationship between the permeability and the porosity $K(\phi)$, between the relative permeabilities and the water saturation $k_{rg}(S_w)$; $k_{rw}(S_w)$, and between the capillary pressure and the water saturation $P_c(S_w)$ (collapsed to a function $J(S_w)$, as described earlier). As illustrated in Fig. 4, each of these relationships has an associated uncertainty, given by

$$\ln K = 52.54\phi - 6.47 \pm 1.03, \tag{11}$$

$$k_{rw} = k^e_{rw} e^{-(A\pm 1.8)R^{-L}_w}, \tag{12}$$

$$k_{rg} = k^e_{rg} e^{-(B\pm 0.9)R^{M}_w}, \tag{13}$$

$$J(S) = S^{*\,-1/\lambda}_w \times (1 \pm 0.2), \tag{14}$$

where the $\pm$ figures are one standard deviation, either additive or multiplicative. Any attempt to describe these properties should be accompanied by an assessment of their uncertainty on the results. Therefore, as a first step towards quantifying uncertainty, in addition to using mean values in our model for capillary trapping, we also used these standard deviation values to estimate upper and lower bounds on our predictions.

4. Flow simulation

The following flow simulations were carried out using the numerical simulator CMG IMEX^{TM} to model CO_2 sequestration and subsequent trapping IMEX (2000). CMG IMEX is a fully implicit, finite volume, finite difference, isothermal immiscible multiphase flow simulator IMEX (2000); Jackson and Krevor (2020). Grid dimensions of 0.5 cm in the flow direction were chosen following a grid refinement study to determine the grid resolution needed to minimise numerical diffusion, which would otherwise artificially smear out the capillary heterogeneity trapping. Each geological model represented a 1D vertical column through the aquifer. The system parameters (Table 1), along with capillary pressure, relative permeability, porosity-permeability and pore-scale initial-residual saturation relationships (Section 2), were defined based on experimental results Jackson and Krevor (2020).

The inlet boundary condition was defined by an injection well with a constant flow rate at the bottom of the domain, and a production well at the top enforcing a constant pressure outlet boundary condition. The simulation was split and run in separate drainage and imbibition steps. The reservoir was initially fully water saturated. First, 100% CO_2 was injected at a constant rate into the bottom of the domain for 1.5 pore volumes, to simulate drainage in a vertical section far from the well.

Fluid was produced from the top to ensure voidage replacement. The final saturation and pressure conditions at the end of drainage were stored and formed the initial conditions at the start of the imbibition process. Next, brine was injected into the bottom of the domain for 1.5 pore volumes, at the same rate CO_2 was injected previously, to mimic brine imbibition. Again, fluid was produced from the top of the domain at the same rate as injected. The conceptual picture underlying the models relevance within a field scale storage site is described in the Supporting Information S4.

4.1. Hysteresis

Constitutive macroscopic properties exhibit hysteresis between drainage and imbibition, resulting from differences in pore-scale mechanisms depending on the displacement pathway Jackson and Krevor (2020). Capillary trapping, on the pore and facies scale, depends on the hysteretic nature of properties including capillary pressure and relative permeability, whose spatial variation is determined by geological heterogeneity Gershenzon et al. (2014). For imbibition processes starting from an intermediate saturated state, it is necessary to account for relative permeability and capillary pressure hysteresis. Hysteresis is employed through the Killough interpolation method, with curvature parameter $\epsilon = 0.1$ chosen to best represent hysteresis in typical sandstones Jackson et al. (2020); Killough (1976).

The modelling of hysteresis was limited to the imbibition displacement for computational efficiency, as solving with hysteresis may lead to numerical instability due to small saturation fluctuations Jackson and Krevor (2020). The 1D drainage simulation saturations were equivalent if hysteresis was included, as primary drainage occurs. Pore-scale residual trapping was represented using the Land trapping model Land (1968) with trapping parameter $C = 1.7$ as per the core-scale experimental data (Fig. 2), unless otherwise specified. CO_2 relative permeability hysteresis was included, necessary to capture pore-scale residual trapping processes. Wetting-phase relative permeability hysteresis was not modelled as it is generally much smaller than the non-wetting phase hysteresis Jerauld and Salter, 1990; Juanes et al. (2006), and is typically not observed in water wet sandstone rocks Jackson et al. (2020). The base simulations did not include capillary pressure hysteresis, this was evaluated separately (see Section 5.3).

4.2. Imbibition capillary pressure

The representation of capillary entry pressure in the capillary pressure - saturation model may have a large impact when modelling CO_2 storage mechanisms. Li et al (2013) show that representing the capillary pressure curve through either the Brooks-Corey or van Genuchten model has important consequences for simulating CO_2 solubility trapping Li et al. (2013).

The form of the imbibition capillary pressure curve, and especially the magnitude of the imbibition threshold pressure, has a leading order impact on the capillary heterogeneity trapped saturation also. As drainage capillary pressure is expected to be greater than that measured for imbibition Bech and Frykman, 2018, simulations only considering the drainage capillary pressure relationship over-estimate capillary heterogeneity trapping within the system and need to be corrected.

Due to experimental limitations, the imbibition capillary pressure - saturation relationship is often unknown Zahasky and Benson (2019), as is the case for the Captain Sandstone. In lieu of an experimentally determined relationship, the effect of two functional forms for the imbibition capillary pressure-saturation relationship from literature

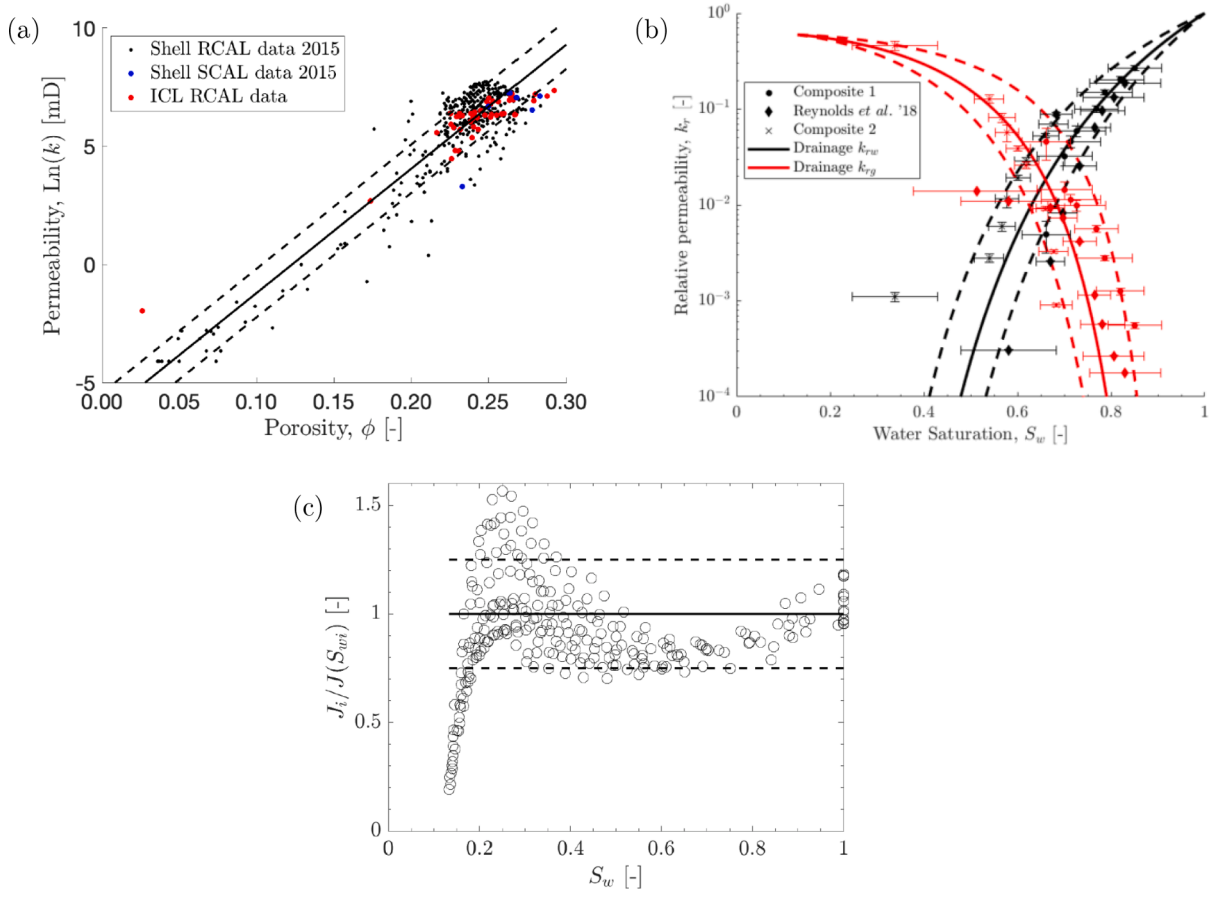

Fig. 4. Different sources of uncertainty in the various relationships used for reservoir modelling. (a) Relationship between porosity ϕ and permeability K. (b) Relationship between relative permeability k_r and water saturation S_w. (c) Relationship between capillary pressure P_c and water saturation S_w.

Jackson et al. (2020); Sedaghat and Azizmohammadi (2019) were evaluated (see Figure S7 in the Supporting Information),

$$P_c^{st} = P_s\left(\frac{S_w - S_{wirr}}{1 - S_{wirr} - S_{CO2,r}}\right)^{-\frac{1}{\lambda_s}}, \tag{15}$$

$$P_c^{mob} = P_{ci}\left(\left(1 - S^*_{CO2,c}\right)^{-\frac{1}{\lambda}} - 1\right) + P_s, \tag{16}$$

where P_c^{st} is the imbibition capillary pressure standardised to the maximum residual CO_2 saturation, $S_{CO2,r}$ Sedaghat and Azizmohammadi (2019). P_s is the imbibition threshold pressure and λ_s is the updated Brooks Corey parameter calculated based on system parameters to produce drainage and imbibition bounding curves which meet at S_{wirr}. P_c^{mob} is the imbibition capillary pressure calculated from the mobile, connected CO_2 saturation $S^*_{CO2,c}$ determined from residual trapping relationships Jackson et al. (2020). P_{ci} can be found through equating the drainage and imbibition capillary pressures at the turning point saturation, as outlined in Pini and Benson (2017).

The imbibition threshold pressure P_s is often unknown for the system of interest. The experimentally derived drainage capillary entry pressure P_e was scaled to each layer's porosity and permeability using the Leverett-J function Eq. 4). We tested the impact of assuming both P_s is equal to P_e ($P_s = P_e$) and P_s to be a constant fraction of the drainage capillary entry pressure ($P_s = P_e/3$). Experimental data Raeesi et al. (2014) suggests the macroscopic capillary pressure - saturation relationship has a finite value at the non-wetting phase residual saturation. The magnitude of P_s is key to calculating the capillary heterogeneity trapped saturation, it has a leading impact on the capillary pressure continuity boundary condition which results in capillary heterogeneity trapping Duijn et al. (1995). Capillary pressure functions described by Van Genuchten models do not result in capillary heterogeneity trapping, due to the omission of a threshold pressure Duijn and De Neef (1996); Gershenzon et al. (2016). A threshold pressure is needed if capillary heterogeneity trapping is to be observed, otherwise there is no capillary pressure barrier to flow and hence no saturation build up. Simulations were carried out on a single realisation of the Captain sandstone with the imbibition capillary pressure curves outlined (Eqs. (15) and (16), considering both $P_s = P_e$ and $P_s = P_e/3$.

4.3. Calculating capillary heterogeneity trapped saturation

The capillary heterogeneity trapped saturation was calculated as the difference between the final saturation observed on imbibition and that calculated as a result of pore-scale residual trapping (Eq. 1), this reflects the additional trapping due to heterogeneity. The average saturations were calculated as porosity weighted averages, as each grid cell has the same thickness. The proportion of trapping resulting from capillary heterogeneities was quantified through Eq. (17).

$$\% = \frac{\text{System average capillary heterogeneity trapped saturation}}{\text{System average total trapped saturation}} \times 100\% \tag{17}$$

5. Results

5.1. Capillary heterogeneity trapping in the base model

The results in Fig. 5 show a heterogeneous saturation is observed at the end of the drainage process, due to capillary entry pressure variations within the system. As the pore-scale residual saturation is dependant on the initial saturation prior to brine imbibition, the residual saturation is observed also to be heterogeneous. The final saturation observed at the end of the imbibition process is greater than that trapped by pore-scale residual mechanisms alone due to the impact of capillary heterogeneity trapping. On both drainage and imbibition, the capillary pressure distribution mitigates discontinuities in capillary pressure resulting from discontinuous capillary entry pressure at the layered heterogeneities (see Supporting Information S6). The capillary heterogeneity trapped saturation builds up behind regions of high entry pressure, a consequence of capillary pressure and flux continuity conditions in the system. The capillary heterogeneity trapped saturation remains stable for many pore volumes of brine injected, establishing itself as a long term trapping mechanism rather than a transient effect.

The impact of rate is shown in Fig. 6. An inverse relationship between rate of brine imbibition and proportion of capillary heterogeneity trapping (Eq. 17) is observed. Low flow rates correspond with low values of the capillary number Krevor et al. (2011). Hence, to maintain flux continuity the distribution of CO_2 saturation at the heterogeneity builds up over a greater distance, resulting in a greater proportion of CO_2 trapped. The 100 different geological realisations result in scatter in the observed % capillary heterogeneity trapped value, which ranges from 4.9±0.8 at low flow rates to 1.5±0.2 at high flow rates, where the ± are one standard deviation. An uncertainty of approximately 33% is associated with 2 standard deviations over all rates. This demonstrates the amount of capillary heterogeneity trapping in a system cannot be predicted exactly, but will instead fall within a range resulting from the geological uncertainty. This highlights the impact of different geological realisations, and therefore layer width, layer ordering and permeability of layers, on the proportion of capillary heterogeneity trapping within the system.

5.2. Impacts of geological and petrophysical uncertainty

Based on the analysis in Section 3.3, simulations were performed to test the impact of one standard deviation uncertainty in the empirical $K(\phi)$, $J(S)$ and $k_r(S)$ relationships Eq. (11)–(14). In addition, the implications of modelling narrow layers with thicknesses below the wireline logging tool resolution were tested by sampling layer thicknesses from a uniform distribution of 0–5% total system thickness. Fig. 7 displays the simulation results accounting for petrophysical uncertainty over different rates, repeated for 20 geological realisations. The results show that accounting for uncertainty in empirical relationships and wireline log measurements can significantly alter the proportion of capillary heterogeneity trapping expected within the system.

Fig. 7a shows the impact of combining uncertainty in the empirical relationships on the capillary heterogeneity trapped saturation. One standard deviation of uncertainty in the $J(S)$, $k_{rg}(S)$ and $k_{rw}(S)$ relationships are combined as so to produce the maximum and minimum amounts of capillary heterogeneity trapping respectively (see Supporting Information S7 for errors resulting from each relationship separately). The mean proportion of capillary heterogeneity trapping over 20 realisations could be up to three times larger or three times smaller than in systems considering no uncertainty in the empirical relationships. Fig. 7b demonstrates the uncertainty when narrow layers, below the wireline log resolution, are accounted for. The mean proportion of capillary heterogeneity trapping over 20 realisations is only approximately 1.1 times greater when layers below 1% of the system height are considered. The results of Fig. 7 show that the uncertainty in the empirical relationships has a greater impact than the uncertainty resulting from the wireline log resolution. The uncertainty due to multiphase petrophysical properties is comparable to the uncertainty resulting from brine imbibition rate and different geological realisations.

5.3. Impacts of capillary pressure hysteresis

Fig. 8 shows the proportion of capillary heterogeneity trapping within the Captain Sandstone is typically reduced when capillary pressure hysteresis is accounted for. The amount of capillary heterogeneity trapping within the system is observed to vary between 30% to 100% of

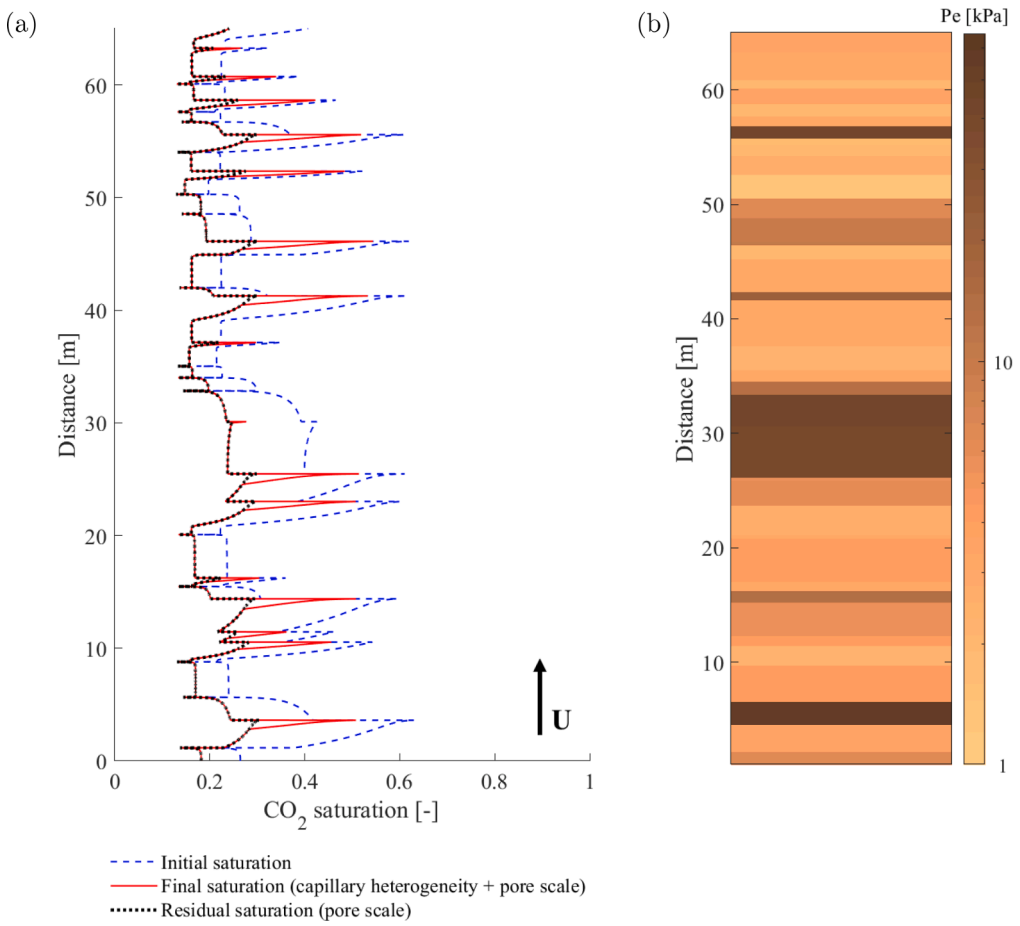

Fig. 5. (a.) The saturation profile with depth for a single geological realisation of the base model, with brine imbibition rate U 0.001 m/day. The initial saturation prior to imbibition, pore-scale residual saturation and final saturation at the end of the imbibition process are shown. For this realisation, the proportion of trapped saturation due to capillary heterogeneities is 5.8%. (b.) Capillary entry pressure variations with depth for this 1D realisation.

that trapped when no hysteresis is modelled, dependant on the functional form of the imbibition capillary pressure curve implemented. These results confirm simulations run with no hysteresis should be taken as an upper bound for the proportion of capillary heterogeneity trapping within a system. This work suggests a correction factor of between 0.3 - 1 (i.e. no correction) is needed to correct for over-estimations in systems where capillary pressure hysteresis has not been included.

Capillary heterogeneity trapping is observed to have a key dependency on the imbibition threshold pressure (Fig. 8). A decrease in imbibition threshold pressure lowers the ratio of capillary forces in the system, resulting in a decrease in trapping. All functional forms of the imbibition capillary pressure curve result in the same inverse trend with rate, demonstrating the trend is universal across different capillary pressure relationships.

5.4. *Consequences for initial-residual saturation relationship*

The analysis in the following section considers the relative capillary heterogeneity trapping between simulations run over different brine imbibition rates and Land trapping parameters. Due to long simulation run times and the unknown form of the imbibition capillary pressure curve, we do not consider capillary pressure hysteresis in this section. This is akin to maximising the capillary heterogeneity trapping (Fig. 8).

Fig. 9 shows the results in terms of initial-residual saturation plots. Deviations from the pore-scale residual Land trapping model result from capillary heterogeneity trapping. Fig. 9a demonstrates the impact of brine imbibition rate, with lower rates resulting in larger deviations due to increased capillary heterogeneity trapping. In order to maintain capillary pressure continuity within a heterogeneous system, capillary pressure gradients form downstream of high capillary entry pressure layers, resulting in a build up in CO_2 saturation. In Fig. 9a each data point represents the saturation in an individual grid cell, with saturation gradients caused by capillary heterogeneities forming lines of points deviating from the pore-scale relationship. The porosity weighted average saturation is calculated for each homogeneous layer, as shown in Fig. 9b. It is observed that the layers with no capillary heterogeneity trapping exhibit behaviour equivalent to the pore-scale residual trapping relationship.

Capillary heterogeneity trapping may be an explanation for the scatter observed in initial-residual core floods Ni et al. (2019) Reynolds et al., 2018, influencing the choice of trapping parameter extracted from experimental data (e.g. Fig. 2). The average trapping parameter, commonly extracted from experimental data, may also represent the impact of capillary heterogeneity trapping in the core, not just the pore-scale residual trapping mechanism alone. The average trapping parameter may actually be an effective or upscaled trapping parameter, incorporating capillary heterogeneity below the experimental representative elementary volume (REV). The impact of rate on capillary heterogeneity trapping, as observed in Fig. 9a, indicates the average Land trapping parameter is a function of rate and thus experimental conditions should be representative of reservoir conditions. Further research is needed to experimentally determine the rate dependency of residual trapping parameters.

We tested the impact of assuming a maximum experimental Land trapping parameter, describing the minimum pore-scale residually trapped saturation, with any additional trapping attributed to capillary

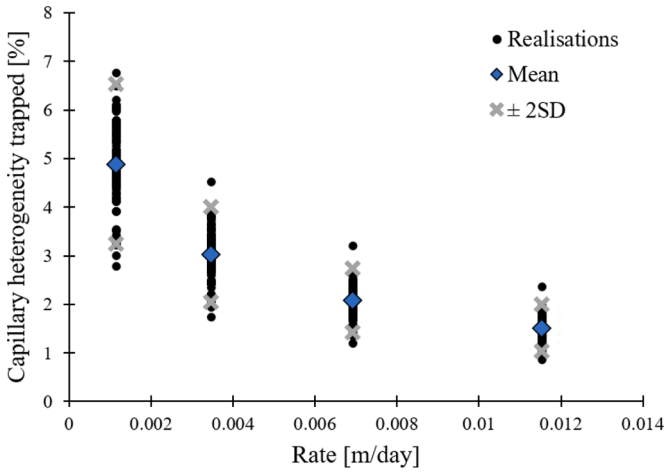

Fig. 6. The proportion of capillary heterogeneity trapping within the system is plotted as a function of brine imbibition rate, an inverse relationship is observed. 100 different geological realisations result in a spread in the proportion of capillary heterogeneity trapping observed.

heterogeneities Reynolds et al., 2018. Fig. 10 demonstrates the importance of extracting either the average or maximum Land trapping parameter from experimental data (Fig. 2a) on field-scale simulations. The results from field-scale simulations using Land trapping parameter (a.) C=1.7 (experimental average) and (b.) C=2.8 (experimental maximum), are overlaid with plug-scale experimental data. As shown in Fig. 10b, modelling the field-scale Captain Sandstone system with the maximum experimental core plug Land trapping parameter, C=2.8, results in a trapping relationship which better agrees with the core plug experimental data. All the core data lies on or above the Land trapping curve. We suggest that this is a more physically realistic model based on the hypothesis that the maximum Land trapping curve represents the pore-scale residual trapping and residual saturations above the Land curve are due to additional capillary heterogeneity trapping.

Models using the maximum Land trapping parameter result in a higher proportion of capillary heterogeneity trapping in the system than originally assumed using the average experimental core plug Land trapping parameter. Table 2 demonstrates, for the rates used, the proportion of capillary heterogeneity trapping is a factor of 2 - 3 times greater when the experimental maximum Land trapping parameter is employed, relative to utilizing the average Land trapping parameter in the simulations.

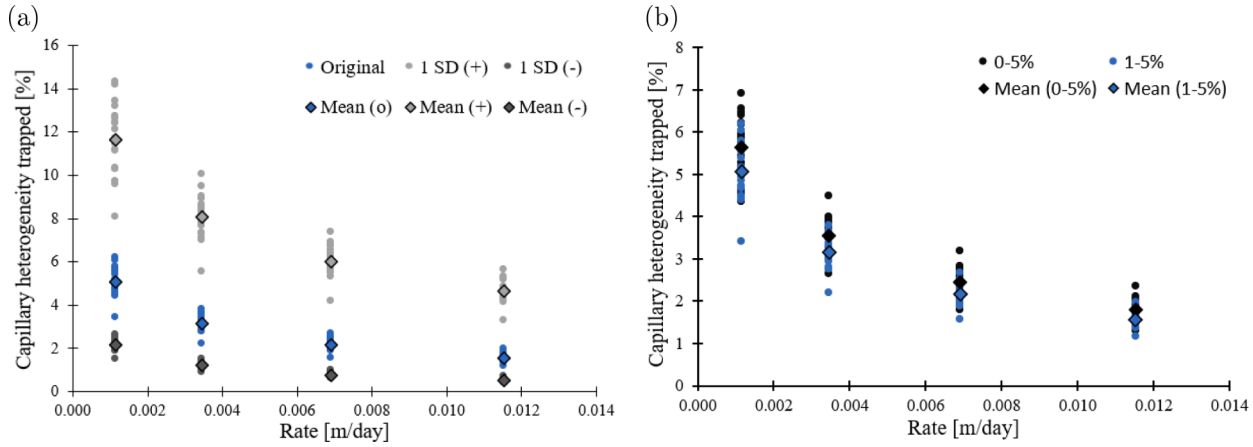

Fig. 7. The proportion of trapping resulting from capillary heterogeneities as a function of rate, repeated for 20 geological realisations. (a.) One standard deviation uncertainty in the empirical relationships $J(S)$, $k_{rg}(S)$ and $k_{rw}(S)$ are combined to produce maximum (+) and minimum (-) proportions of capillary heterogeneity trapping, compared to the original system (o) where no uncertainty in the empirical relationships is considered. (b.) Layer thicknesses below 1% system thickness are sampled.

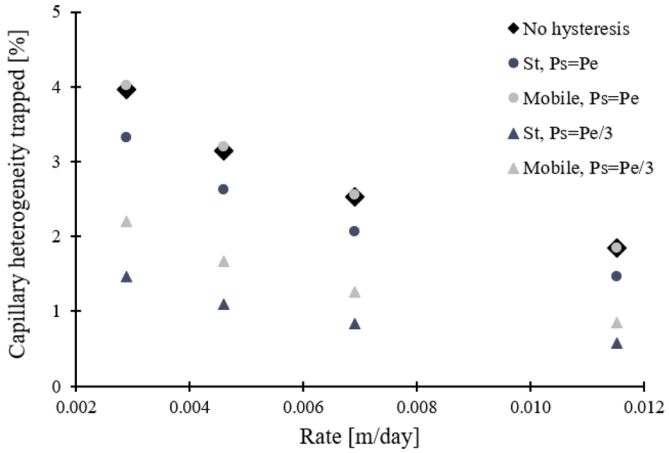

Fig. 8. Impact of brine imbibition rate on the proportion of capillary heterogeneity trapping within the Captain Sandstone for different imbibition capillary pressure curves. Simulations where capillary pressure hysteresis is accounted for typically demonstrate lower proportions of capillary heterogeneity trapping.

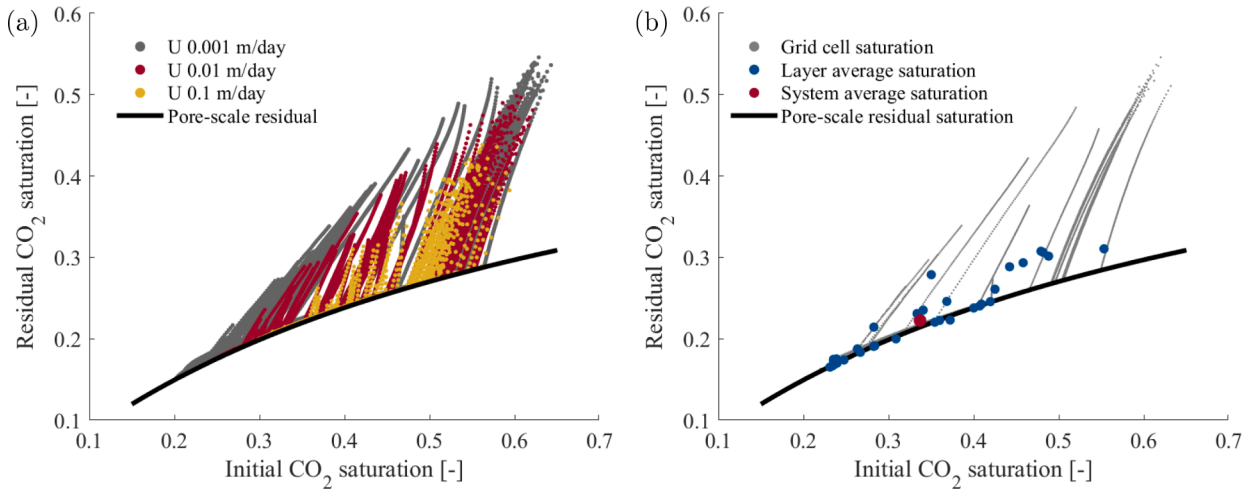

Fig. 9. (a.) The final saturation observed on imbibition is plotted against the initial saturation prior to imbibition for 5 geological realisations, over different rates. Deviations from the Land pore-scale residual trapping model are observed due to capillary heterogeneity trapping, with increased deviations at lower rates. (b.) Layer average and system average initial-residual saturations are displayed, in addition to individual grid cell saturations, for 1 geological realisation at a rate 0.001m/day.

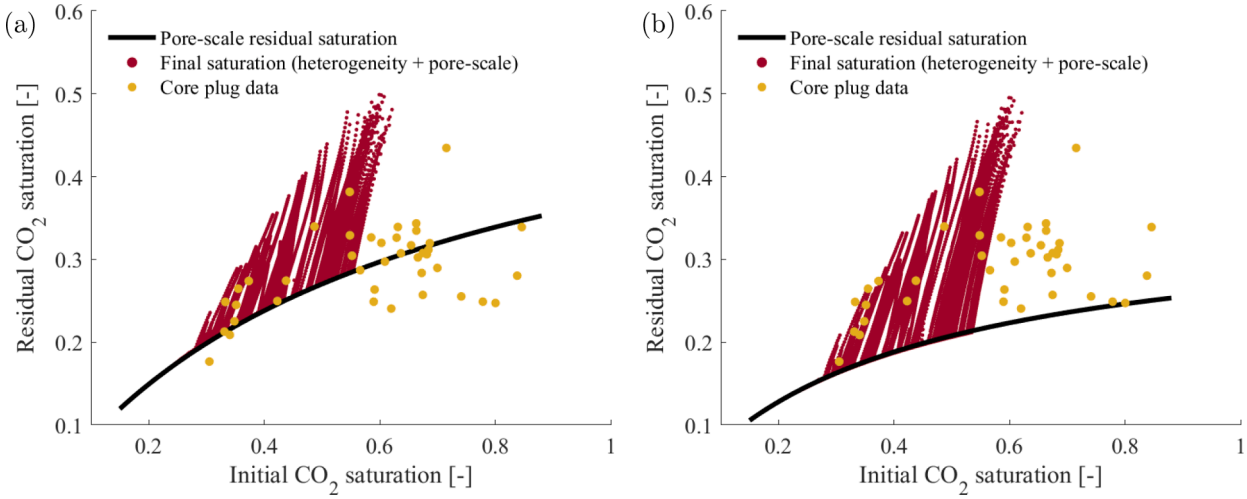

Fig. 10. Initial-residual saturation relationships for 5 geological realisations, simulated with a rate of 0.01 m/day. The final saturation on imbibition (capillary heterogeneity + pore-scale) and the pore-scale residual saturation from simulation are overlaid with the experimental core plug data from Fig. 2a. The simulations were modelled with Land trapping parameter (a.) $C = 1.7$ and (b.) $C = 2.8$.

Table 2
The proportion of capillary heterogeneity trapped saturation in the system, averaged over 5 geological realisations. The results are demonstrated for three rates and two trapping parameters C used in the simulation.

Rate [m/day]	% ($C = 1.7$)	% ($C = 2.8$)
0.1	0.3	1
0.01	1.7	4.2
0.001	5.3	10.5

These results should be used to compare the relative difference in capillary heterogeneity trapping between simulations ran using different Land trapping parameters. As these simulations do not account for capillary pressure hysteresis the amount of capillary heterogeneity trapping should be considered a maximum and may be as low as 30% of these values depending on the shape of the imbibition curve. Additionally, considering the impact of petrophysical uncertainty, the amount of capillary heterogeneity trapping may vary as outlined in Section 5.2.

6. Discussion

This paper outlines a workflow to create heterogeneous decametre-scale models from core-scale experimental data, applied to the Captain D Sandstone. Vertical flow upwards through layered 1D Captain Sandstone realisations was simulated to mimic a CO_2 migration and trapping project. On imbibition, the resulting saturation distribution displayed a build-up in capillary heterogeneity trapped saturation upstream of regions of high capillary entry pressure. Different geological realisations were generated to demonstrate the impact of possible heterogeneous layered environments on capillary heterogeneity trapping. The uncertainty from the underlying empirical relationships, wireline log resolution, geological realisation and imbibition flow rate were evaluated, emphasising that the exact proportion of capillary heterogeneity trapping cannot be predicted by modelling but rather the bounds of the trapping should be estimated from the uncertainties inherent in the model. We have shown it is important to account for the uncertainty in wetting phase relative permeability, brine imbibition rate and geological realisation as they have the greatest impact on the proportion of capillary heterogeneity trapping in the system. Uncertainties in wireline log resolution and certain empirical relationships such as the porosity-

permeability relationship have minimal impact on capillary heterogeneity trapping in this case, and may be neglected.

The consequences of omitting capillary pressure hysteresis were evaluated through testing different forms of the imbibition capillary pressure - saturation relationship. The results show, depending on the imbibition capillary pressure curve used in simulations, failure to model capillary pressure hysteresis may overestimate the capillary heterogeneity trapped saturation by up to 3 times. Further work should be carried out to experimentally determine the imbibition capillary pressure curve for the Captain Sandstone, and other target storage sites, in order to reduce the uncertainty associated with this relationship.

The resulting saturation distributions from flow simulations run on models representative of the Goldeneye field demonstrate deviations from the pore-scale residual Land trapping relationship, which is a consequence of capillary heterogeneity trapping. The impacts of extracting the average Land trapping parameter from core flood initial - residual saturation relationships, and using in field-scale simulations, were shown. Further work is needed to evaluate experimentally the impact of system conditions (e.g. rate) on the average Land trapping parameter and how this influences multi-level upscaling approaches. This paper highlights the potential importance of capillary heterogeneity trapping when assessing the storage security of target field storage sites and the need to develop methods to upscale that trapping. Although this work focused on a case study of the Captain Sandstone, the findings are applicable beyond this reservoir.

We were unable to find a correlation between the proportion of capillary heterogeneity trapping in the system and the dimensionless heterogeneity factor defined in Li and Benson, 2015. This corroborates the field-scale results of Dance and Paterson (2016) who found little or no correlation between residual trapping characteristics and system properties such as porosity, permeability and sorting. Identifying an upscaled parameter indicative of the amount of capillary heterogeneity trapping in a field-scale site should be the subject of future investigation, in order to quickly estimate the impact of heterogeneity on trapping within target storage sites.

This analysis is limited most significantly by its 1D nature, and assumption of only one facies. Although this has direct application in systems such as layer-cake structures (Fig. 5b) Kjonsvik et al. (1994), higher dimensions are required to model a more realistic reservoir system. 2D and 3D systems allow for the bypass of fluid around heterogeneities which do not span the whole system The IPCC special report on carbon dioxide capture and storage (2006). However, this analysis provides an initial estimate of the maximum expected capillary heterogeneity trapping and the impact of petrophysical and geological uncertainty. In addition, a constant flow rate is assumed, which does not account for flow rate variations and draws into question the most appropriate choice of flow rate for the system. Due to pressure gradients, the drainage flow rate is expected to vary with distance from the injection well Jackson and Krevor (2020), with the imbibition flow rate even less well constrained. The clear impact of rate on capillary heterogeneity trapping has been demonstrated, yet the brine imbibition rate may vary over many orders of magnitude, making it difficult to predict an ubiquitous value for the proportion of capillary heterogeneity trapping within a target storage site.

7. Conclusion

This paper highlights the importance of incorporating capillary heterogeneity and geological uncertainty into workflows modelling and predicting CO_2 trapping. Key outstanding uncertainties were investigated including the impact of capillary pressure hysteresis and geological uncertainty on capillary heterogeneity trapping. The research used laboratory and field data from the Captain D sandstone, but the insights apply to all aquifers with capillary heterogeneity. By building models based on site specific data, a target field setting, the Goldeneye field of the Captain Sandstone, is evaluated. We find within the experimental uncertainty resulting from petrophysical characterisation, field geology and variable flow conditions, the proportion of trapping resulting from capillary heterogeneities is expected to vary between 0% and 14% for the Captain D Sandstone. By modelling the system with the maximum experimental Land trapping parameter, as recommended through this paper, the proportion of capillary heterogeneity trapping could be three times as large. Incorporating capillary pressure hysteresis is shown to typically reduce the amount of capillary heterogeneity trapping, by up to 70% for the flow conditions and relationships tested. Appropriate upscaled measures from core analysis should be considered when accounting for capillary heterogeneity at the field scale.

Declaration of Competing Interest

The authors declare that they have no known competing financial interests or personal relationships that could have appeared to influence the work reported in this paper.

Acknowledgements

We gratefully acknowledge sponsorship from EPSRC and BP (Grant Number EP/R513052/1). We acknowledge Computer Modelling Group (CMG) for providing access to IMEX. Great thanks to Alistair Jones and Tony Espie for insightful conversations.

Supplementary material

Supplementary material associated with this article can be found, in the online version, at doi:10.1016/j.ijggc.2021.103511. Data associated with this work is hosted on the NERC EDS National Geoscience Data Centre at https://doi.org/10.5285/8420c937-dbf0-477b-8fc2-921589a7f474<https://nam11.safelinks.protection.outlook.com/?url=https%3A%2F%2Fdoi.org%2F10.5285%2F8420c937-dbf0-477b-8fc2-921589a7f474)&data=04%7C01%7Cs.singh.7%40elsevier.com%7Cfb8f15851360496b053508d9a8597909%7C9274ee3f94254109a27f9fb15c10675d%7C0%7C0%7C637725924557409383%7CUnknown%7CTWFpbGZsb3d8eyJWIjoiMC4wLjAwMDAiLCJQIjoiV2luMzIiLCJBTiI6Ik1haWwiLCJXVCI6Mn0%3D%7C3000&sdata=9xKORFhm%2Ftuio0GxQ9p9mdTuRa2chZfvOqdWWaYunws%3D&reserved=0>.

References

Bech, N., Frykman, P., 2018. Trapping of buoyancy-driven CO_2 during imbibition. Int. J. Greenhouse Gas Control 78, 48–61. https://doi.org/10.1016/j.ijggc.2018.06.018.

Benson, et al., 2012. Chapter 13: carbon capture and storage. Global Energy Asssessment 993–1068.

Benson, S., Pini, R., Reynolds, C., Krevor, S., 2013. Global CCS institute targeted report no. 2: relative permeability analyses to describe multi-phase flow in CO_2 storage reservoirs. 51.

Blondes, M., Brennan, S., Merrill, M., et al., 2013. National Assessment of Geologic Carbon Dioxide Storage Resources – Methodology Implementation. U.S. Geological Survey Open-File Report.[Online]. Available: https://pubs.usgs.gov/of/2013/1055/OF13-1055.pdf

Boom, W., Doe, P., Goodyear, S., Cable, A., Mogford, D., 2012. SCAL Programme for Goldeneye CO_2Storage. 3rd EAGE CO_2 Geological Storage Workshop: Understanding the Behaviour of CO_2 in Geological Storage Reservoirs, pp. 26–28. https://doi.org/10.3997/2214-4609.20143830.

Brooks, R.H., Corey, A.T., 1964. Hydraulic properties of porous media. Hydrology Papers 3, 1–27.

Chadwick, R.A., Noy, D., Arts, R., Eiken, O., 2009. Latest time-lapse seismic data from Sleipner yield new insights into CO_2 plume development. Energy Procedia 1, 2103–2110. https://doi.org/10.1016/j.egypro.2009.01.274.

Chierici, G.L., 1984. Novel relations for drainage and imbibition relative permeabilities. Society of Petroleum Engineers journal 24, 275–276. https://doi.org/10.2118/10165-PA.

Dance, T., Paterson, L., 2016. Observations of carbon dioxide saturation distribution and residual trapping using core analysis and repeat pulsed-neutron logging at the CO_2CRC Otway site. Int. J. Greenhouse Gas Control 47, 210–220. https://doi.org/10.1016/j.ijggc.2016.01.042.

Devroye, L., 1986. Non-uniform random variate generation. Springer-Verlag, New York. Ch. Section 2.2. Inversion by numerical solution of F(X) = U

Duijn, C.J.V., Molenaar, J., De Neef, M.J., 1995. The effect of capillary forces on immiscible two-phase flow in heterogeneous porous media. Transp Porous Media 21, 71–93. https://doi.org/10.1007/BF00615335.

Duijn, C. V., De Neef, M., 1996. Self-similar profiles for capillary diffusion driven flow in heterogeneous porous media. Vol. 9601, p. 24.

Gershenzon, N.I., Ritzi, R.W., Dominic, D.F., Mehnert, E., Okwen, R.T., 2016. Comparison of CO_2 trapping in highly heterogeneous reservoirs with brooks-corey and van genuchten type capillary pressure curves. Adv Water Resour 96, 225–236. https://doi.org/10.1016/j.advwatres.2016.07.022.

Gershenzon, N.I., Ritzi, R.W., Dominic, D.F., Mehnert, E., Okwen, R.T., Patterson, C., 2017. CO_2Trapping in reservoirs with fluvial architecture : sensitivity to heterogeneity in permeability and constitutive relationship parameters for different rock types. Journal of Petroleum Science and Engineering 155, 89–99. https://doi.org/10.1016/j.petrol.2016.09.008.

Gershenzon, N.I., Soltanian, M., Ritzi, R.W., Dominic, D.F., 2014. Influence of small scale "heterogeneity on CO_2 trapping processes in deep saline aquifers. Energy Procedia 59, 166–173. https://doi.org/10.1016/j.egypro.2014.10.363.

IMEX, 2000. Advanced oil/gas reservoir simulator version 2000 user's guide. Computer Modelling Group LTD.

Jackson, S., Lin, Q., Krevor, S., 2020. Representative elementary volumes, hysteresis and heterogeneity in multiphase flow from the pore to continuum scale. Water Resour Res 1–33. https://doi.org/10.1029/2019wr026396.

Jackson, S.J., Agada, S., Reynolds, C.A., Krevor, S., 2018. Characterizing drainage multiphase flow in heterogeneous sandstones. Water Resour Res 54, 3139–3161. https://doi.org/10.1029/2017WR022282.

Jackson, S.J., Krevor, S., 2020. Small-scale capillary heterogeneity linked to rapid plume migration during CO_2 storage. Geophys Res Lett. https://doi.org/10.1029/2020GL088616.

Jerauld, G., Salter, S., 1990. The effect of pore-structure on hysteresis in relative permeability and capillary pressure: pore-level modeling. Transp Porous Media 5, 103–151.

Jin, M., Mackay, E., Akhurst, M., Hitchen, K., Quinn, M., 2012. Evaluation of the CO_2Storage Capacity of the Captain Sandstone Formation (SPE 154539). 74th European Association of Geoscientists and Engineers Conference and Exhibition 2012 Incorporating SPE EUROPEC, pp. 134–150. https://doi.org/10.2118/154539-ms.

Juanes, R., Spiteri, E.J., Orr, F.M., Blunt, M.J., 2006. Impact of relative permeability hysteresis on geological CO_2 storage. Water Resour Res 42, 1–13. https://doi.org/10.1029/2005WR004806.

Killough, J.E., 1976. Reservoir simulation with history-dependent saturation functions. Soc Pet Eng AIME J 16, 37–48.

Kjonsvik, D., Doyle, J., Jacobsen, T., Jones, A., 1994. Effects of sedimentary heterogeneities on production from a shallow marine reservoir - what really matters? Proceedings European Petroleum Conference, pp. 27–40. https://doi.org/10.2523/28445-ms.

Krevor, S., Blunt, M.J., Benson, S.M., et al., 2015. Capillary trapping for geologic carbon dioxide storage - from pore scale physics to field scale implications. Int. J. Greenhouse Gas Control. https://doi.org/10.1016/j.ijggc.2015.04.006.

Krevor, S.C., Pini, R., Li, B., Benson, S.M., 2011. Capillary heterogeneity trapping of CO_2 in a sandstone rock at reservoir conditions. Geophys Res Lett 38, 1–5. https://doi.org/10.1029/2011GL048239.

Krevor, S.C., Pini, R., Zuo, L., Benson, S.M., 2012. Relative permeability and trapping of CO_2 and water in sandstone rocks at reservoir conditions. Water Resour Res 48, 1–16. https://doi.org/10.1029/2011WR010859.

Land, C.S., 1968. Calculation of imbibition relative permeability for two- and three-phase flow from rock properties. Society of Petroleum Engineers Journal 8, 149–156. https://doi.org/10.2118/1942-pa.

Leverett, M., 1940. Capillary behavior in porous solids. Petroleum Technology 152–169. https://doi.org/10.2118/941152-G.

Li, B., Tchelepi, H.A., Benson, S.M., 2013. The influence of capillary entry-pressure representation on CO_2 solubility trapping. Energy Procedia 37, 3808–3815. https://doi.org/10.1016/j.egypro.2013.06.277.Issn: 18766102

Li, B., Benson, S.M., 2015. Influence of small-scale heterogeneity on upward CO_2 plume migration in storage aquifers. Adv Water Resour 83, 389–404. https://doi.org/10.1016/j.advwatres.2015.07.010.

Li, X., Boek, E., Maitland, G.C., Trusler, J.P., 2012. Interfacial tension of (brines + CO_2): (0.864 NaCl + 0.136 KCl) at temperatures between (298 and 448) K, pressures between (2 and 50) MPa, and total molalities of (1 to 5) mol kg-1. J Chem Eng Data 57, 1078–1088. https://doi.org/10.1021/je201062r.

Mathias, S.A., Gluyas, J.G., de Miguel, G.J.G.M., Bryant, S.L., Wilson, D., 2013. On relative permeability data uncertainty and CO_2 injectivity estimation for brine aquifers. Int. J. Greenhouse Gas Control 12, 200–212. https://doi.org/10.1016/j.ijggc.2012.09.017.

Metcalfe, R., Thatcher, K., Towler, G., Paulley, A., Eng, J., 2017. Sub-surface risk assessment for the Endurance CO_2 store of the White Rose project, UK. Energy Procedia 114, 4313–4320. https://doi.org/10.1016/j.egypro.2017.03.1578.

Ni, H., Boon, M., Garing, C., Benson, S.M., 2019. Predicting CO_2 residual trapping ability based on experimental petrophysical properties for different sandstone types. Int. J. Greenhouse Gas Control 86, 158–176. https://doi.org/10.1016/j.ijggc.2019.04.024.

Obi, E.O.I., Blunt, M.J., 2006. Streamline-based simulation of carbon dioxide storage in a North Sea aquifer. Water Resour Res 42. https://doi.org/10.1029/2004WR003347.

Pini, R., Benson, S.M., 2013. Simultaneous determination of capillary pressure and relative perme ability curves from core-flooding experiments with various fluid pairs. Water Resour Res 49, 3516–3530. https://doi.org/10.1002/wrcr.20274.

Pini, R., Benson, S.M., 2017. Capillary pressure heterogeneity and hysteresis for the supercritical CO_2/water system in a sandstone. Adv Water Resour 108, 277–292. https://doi.org/10.1016/j.advwatres.2017.08.011.

Raeesi, B., Morrow, N.R., Mason, G., 2014. Capillary pressure hysteresis behavior of three sandstones measured with a multistep outflow-inflow apparatus. V top Vadose Zone J. 13 https://doi.org/10.2136/vzj2013.06.0097.Vzj2013.06.0097

Reynolds, C.A., Blunt, M.J., Krevor, S., 2018. Multiphase flow characteristics of heterogeneous rocks from CO_2 storage reservoirs in the United Kingdom. Water Resour Res 54, 729–745. https://doi.org/10.1002/2017WR021651.

Reynolds, C.A., Krevor, S., 2015. Characterizing flow behavior for gas injection: relative permeability of CO_2-brine and N_2-water in heterogeneous rocks. Water Resour Res 51, 9464–9489. https://doi.org/10.1002/2015WR018046.

Saadatpoor, E., Bryant, S.L., Sepehrnoori, K., 2010. New trapping mechanism in carbon sequestration. Transp Porous Media 82, 3–17. https://doi.org/10.1007/s11242-009-9446-6.

Sedaghat, M.H., Azizmohammadi, S., 2019. Representative-elementary-volume analysis of two-phase flow in layered rocks. SPE Reservoir Evaluation and Engineering 22, 1075–1083. https://doi.org/10.2118/194014-PA.

Shell, 2015. Peterhead CCS project. Tech. Rep. pp. 1–73.

The IPCC special report on carbon dioxide capture and storage, 2006. 1611–1618.

Spence, B., Horan, D., Tucker, O., 2014. The Peterhead-Goldeneye gas post-combustion CCS project. Energy Procedia 63, 6258–6266. https://doi.org/10.1016/J.EGYPRO.2014.11.657.

Tiab, D., Donaldson, E.C., 2016. Chapter 12 - Shale-gas Reservoirs. Petrophysics (Fourth Edition), Fourth edition. Gulf Professional Publishing, Boston, pp. 719–774. https://doi.org/10.1016/B978-0-12-803188-9.00012-7.

Tucker, O., Tinios, L., 2017. Experience in developing the Goldeneye storage permit application. Energy Procedia 114, 7466–7479. https://doi.org/10.1016/j.egypro.2017.03.1880.

Zahasky, C., Benson, S.M., 2019. Spatial and temporal quantification of spontaneous imbibition. Geophys Res Lett 46, 11972–11982. https://doi.org/10.1029/2019GL084532.